Time-Dependent DFT Studies of Metal Core-Electron Excitations in Mn Complexes

Adrian R. Jaszewski, Rob Stranger, and Ronald J. Pace*

Department of Chemistry, Faculty of Science, Australian National University, Canberra ACT 0200, Australia

Received: April 16, 2008; Revised Manuscript Received: August 15, 2008

Time-dependent density functional theory (TDDFT) has been applied to study core excitations from 1s and 2p Mn orbitals in a series of manganese complexes with oxygen and nitrogen donor ligands. The effect of basis set and functional on the excitation energy was evaluated in detail for one complex, $Mn(acac)_2 \cdot (H_2O)_2$. The results obtained for a range of compounds, namely, $[Mn(Im)_6]Cl_2$, $Mn(CH_3COO)_2 \cdot 4H_2O$, $Mn(acac)_3$, $Mn(SALADHP)_2$ and $[Mn(SALPN)O]_2$, show good consistency with the data from X-ray absorption spectroscopy (XAS), confirming the relation between the Mn K-edge energy and the oxidation state of the Mn atom. The energies predicted for 2p core excitations show a dependence on the metal oxidation state very similar to that determined experimentally by 1s2p resonant inelastic X-ray scattering (RIXS) studies for $Mn(acac)_2 \cdot (H_2O)_2$, $Mn(acac)_3$, and $Mn(sal)_2(bipy)$. The reliability of the K-edge energies obtained in the present study indicates that TDDFT can be used in determining the oxidation states of Mn atoms in different computational models of the manganese cluster of photosystem II (PSII).

1. Introduction

An estimated 30−50% of all enzymes[1] must bind one or more metal ions for functional activity. Generally, this requirement arises because of the involvement of metal atoms in the catalytic mechanism or because the bound ions determine or stabilize the protein tertiary or quaternary structure. Metalloenzymes are particularly involved in the various bioenergetic pathways crucial for life, including photosynthesis and respiration.[2] In these cases, the mechanism of catalytic activity can frequently be formulated as a cycle with several intermediate states, characterized by different oxidation states of the metal and/or different structural arrangements around the metal. The structural and electronic changes of the metal center are therefore crucial for understanding the mechanism of the reactions catalyzed by most metalloenzymes. However, despite years of study, many instances of ambiguity remain in relation to both structural and electronic characteristics of the systems involved in very important biochemical processes, such as the interconversion of dihydrogen to protons and electrons by hydrogenases,[3−5] the fixation of nitrogen to generate ammonia by nitrogenases,[6,7] and the oxidation of water by photosystem II (PSII),[8−10] to name only a few.

In this regard, X-ray absorption spectroscopy (XAS),[11] which allows for the characterization of the oxidation state of the protein-bound metal, can be a useful tool in studies of metalloenzymes and has been widely used for this purpose.[12−14] However, the metal X-ray absorption near-edge structure (XANES), which carries information about the oxidation state of the atom, is still not completely understood at a quantitative, theoretical level.[15]

The main focus of this article is to explore the usefulness of time-dependent density functional theory (TDDFT) calculations in the analysis of the edge regions of the X-ray absorption spectra of Mn complexes in various oxidation states. The aim is to develop a reliable methodology, based on established theoretical grounds, for analyzing X-ray absorption spectra of metalloenzymes and, in particular, manganese K-edge regions of X-ray absorption spectra. This project is complementary to our recent DFT computational studies on the structure of the water-oxidizing complex (WOC) of PSII,[16] which addressed the issue of the observed variation in manganese positions in the X-ray diffraction (XRD) experiments.[17−19]

The water-oxidizing center (WOC) in functioning PSII consists of a metal cluster comprising four manganese atoms and one calcium atom. It produces O_2 by a four-step catalytic process in which five intermediate states (S_n with $n = 0-4$) can be identified.[8] On going from S_0 to S_4, one electron is withdrawn from the WOC at each step. However, even when changes in the Mn oxidation state during this cycle are monitored by XAS,[20−26] the data do not provide a clear picture of the exact oxidation state of Mn atoms at each step. In fact, certain experimental results are used to support the idea that a positive charge is created on a ligand(s) rather than on Mn in the $S_2 \rightarrow S_3$ transition.[27] Because the ligand environment, including bridging ligands between the manganese atoms, is not definitively determined even by the most recent X-ray diffraction (XRD) studies,[17−19] a complete analysis of the mechanism of oxidation accumulation within the cluster has yet to be presented.

One method to address these difficulties and learn more about the electronic structure of the Mn_4Ca cluster is to compare the spectroscopic properties of the WOC with those of model manganese compounds with well-determined geometries. Experimental XAS data are available for many manganese systems, from oxides and simple inorganic salts[28,29] to macromolecules containing metal clusters with Mn atoms in different oxidation states linked by oxo bridges.[30,31] As expected, Mn K-edge energies show a strong dependence on the oxidation state of the metal. On going from the 2+ to the 4+ state, the energy of the first inflection point on the rising absorption edge can increase by more than 7 eV.[30] However, this relation is not linear with formal oxidation number, because K-edge energies are dependent on the type of ligands and the ligand-field symmetry as well.[32] The simplest computational parameter expected to give a linear dependence is the effective metal-centered charge,

* Corresponding author. Phone: +61-(0)2-61254546. Fax: +61-(0)2-61258997. E-mail: Ron.Pace@anu.edu.au.

10.1021/jp803286c CCC: $40.75
Published on Web 10/14/2008

obtained by taking into account the charge distribution resulting from the mixing of ligand and metal orbitals,[33] that is, the covalency of the metal−ligand bonds. However, at least computationally, this seems to be an arbitrary approach, if not supported by any reliable charge population analysis, as provided by the Atoms in Molecules (AIM) method,[34] for instance. On the other hand, for a series of manganese oxides studied by 1s2p resonant inelastic X-ray scattering (RIXS),[33] a linear relation was recently observed between the incident energy and the energy transfer, which relate to the excitation energies in K-edge and L-edge absorption spectroscopy, respectively. The results obtained for different manganese complexes generally followed this trend, whereas the S_1 and S_2 states of PSII deviated somewhat from the linear correlation.[33]

The difficulties of direct comparisons between the WOC and model complexes are due not only to the effect of a strong dependence of edge energies on the ligand environment, the latter of which is not well established for the Mn cluster of PSII, but also to the relatively small total change of K-edge energy during S-state advancement. This energy change, as reported by several groups and recently reviewed,[8] is ca. 3 eV between S_0 and S_3. XAS does not discriminate between individual Mn atoms but effectively averages this property of the cluster. If the oxidation state of one Mn atom increases by 1 on going from S_n to S_{n+1}, the observed shift in energy is typically ca. one-fourth of that arising on the single ion, because the remaining three Mn atoms are unchanged. In fact, this change in K-edge energy with S-state advancement is so small that it represents only about twice the variation in the absolute energy for a particular S state determined by different research groups.[8] Such a discrepancy between absolute energy values derives in part from the different ways of defining the edge energy position[35]—by inflection-point, half-height, or integral methods, for instance—and the different methods of calibration or normalization applied.[36] However, the general trend of incremental changes in K-edge energy on going from the S_0 state to the S_3 state is consistent between the different experimental data sets.[8]

In light of recent XRD studies on the structure of PSII[17−19] and extensive electron paramagnetic resonance (EPR), electron−nuclear double resonance (ENDOR), Fourier transform infrared (FTIR), and other spectroscopic investigations of this system,[37−47] a new approach to understanding the electronic and structural properties of the WOC is now feasible. Modern density functional theory (DFT) is capable of successfully modeling electronic and other properties of medium-sized and even large molecules.[48−51] Therefore, it is now possible to construct different models of the Mn_4Ca cluster that incorporate all of the structural constraints observed in the X-ray data while exploring the different modes of ligand binding suggested by a variety of spectroscopic techniques.

The ultimate goal would be to create a comprehensive model that agrees with structural data and satisfactorily explains all of the electronic properties observed experimentally, including the mechanism of water oxidation. In that case, it should be possible to determine the stereochemical and electronic characteristics of the WOC at each particular S state and explain how the geometry and oxidation states of the Mn ions in the cluster change during S-state advancement. An important validation of this model would be the agreement between the oxidation states inferred from the experimental data and those predicted theoretically. Because the exact oxidation state of each Mn atom cannot be definitively determined by the XAS data, any validation would require close agreement between the experimental and calculated values of the K-edge energies in the X-ray absorption spectra. The consistency of the total model with the experimental data would enable an unambiguous determination of the oxidation state of each Mn atom in all S states. The results summarized in this article represent our assessment of using TDDFT as a tool to predict the Mn K-edge and L-edge energies in model compounds.

The 1s and 2p excitation energies are not only challenging to determine experimentally by XAS and RIXS methods, but also difficult to predict theoretically.[52] The high-energy extended X-ray absorption fine structure (EXAFS) region can be described and interpreted successfully within the multiple-scattering (MS) theory, using the so-called muffin-tin (MT) approximation for the shape of the effective potential[15] around the scattering atom. However, MS calculations of the XANES region are more challenging, because, here, the photoexcited electron has little or no excess kinetic energy, so its behavior is strongly influenced by the local potential of the scattering atom and its bonding environment. Therefore, XANES results are much more sensitive to higher-order MS pathways,[53] as well as the details of the scattering potential itself.[54] To fit the XANES region of X-ray absorption spectra of periodic or nonperiodic systems, an approach based on the real-space multiple-scattering (RSMS) formalism with the addition of a self-consistent field exchange-correlation potential has to be used.[55−60] However, even if RSMS theory gives a formally unified treatment of EXAFS and XANES, it is still not completely successful in describing the edge region itself, which is especially sensitive to the atomic and chemical properties of the system. This is particularly important in our intended applications, where uncertainty at even the 1 eV level renders the approach compromised.

A different description of the edge region that is an alternative to the quasiparticle one-electron approach provided by MS theory can be obtained from time-dependent DFT calculations, allowing discussion of the phenomena in terms of the electronic structure of the ground and final states and energy of the excitations. In recent years, the TDDFT methodology[61] has been successfully applied to the simulation of core excitation spectra of simple molecules.[62−64] Larger molecules of biological importance,[65] as well as transition-metal oxides[66] (because of the strong mixing between the metal d and oxygen p levels), represent particularly difficult classes of compounds for theoretical calculations of these and other spectroscopic properties.

Time-dependent DFT can be regarded as a rigorous extension of time-independent DFT to a system, initially in its ground stationary state, that is subjected to a time-dependent perturbation modifying its external potential, v. Analogous to the minimum-energy principle of DFT, a stationary action principle can be derived,[67] leading to the time-dependent equation

$$\left[-\frac{1}{2}\nabla^2 + v(\mathbf{r},t) + \int \frac{\rho(\mathbf{r}',t)}{|\mathbf{r}-\mathbf{r}'|}\,\mathrm{d}\mathbf{r}' + v_{\mathrm{xc}}^{\sigma}(\mathbf{r},t)\right]\psi_{j\sigma}(\mathbf{r},t) = \mathrm{i}\frac{\partial}{\partial t}\psi_{j\sigma}(\mathbf{r},t)$$

where v_{xc}^{σ} is a time-dependent analogue of the exchange-correlation functional from the time independent theory, i.e., a functional of the density as a function of space and time. In the adiabatic limit,[68] it is approximated by the same exchange-correlation potential as in the static case but evaluated using the charge density at time t.

TDDFT can be applied to calculate the dynamic polarizability, $\bar{\alpha}(\omega)$, of a system, which describes the response of the dipole moment to the time-dependent electric field. The poles of the dynamic polarizability, on the other hand, can be used to

determine the electronic excitation spectrum according to the sum-over-states expression

$$\bar{\alpha}(\omega) = \sum_I \frac{f_I}{\omega_I^2 - \omega^2}$$

where ω_I is the energy of the excitation and f_I is the corresponding oscillator strength. In the finite-basis-set implementations of TDDFT,[69] the eigenvalue equation

$$\Omega \vec{F}_I = \omega_I^2 \vec{F}_I$$

which is actually solved, gives the squares of excitation energies, and the corresponding oscillator strengths can be extracted from the F_I eigenvectors.

Because TDDFT formally includes coupling between one-electron excited configurations, it represents an essential improvement over single-particle approaches in the description of the excitation energies. Furthermore, current implementations of TDDFT for the core-electron excitations allow reduction of the complete one-electron excited configuration space to the subspace where only core electrons are excited.[70] This lowers the cost of computations for large systems and allows for the calculation of the excitations of K or L electrons, even for heavy metal atoms. As noted elsewhere,[35] however, a deficiency of any molecular-orbital- (MO-) based approach is that it does not readily permit simulation of the actual XANES edge shape. Only transition energies and probabilities are computed; no account is taken of the real transition line widths or the beginnings of electron backscatter interference effects. Thus, we expect to be able to correlate our computational results only with an experimental "mean edge" (equivalent to "peak center") position. As discussed above, even this is not unique for XANES spectroscopy, with several empirical measures being used.

2. Computational Details

Initial geometries for the molecules (Figure 1) were derived from the XRD structures[71−77] of $Mn(acac)_2 \cdot (H_2O)_2$ (**1**), $[Mn(Im)_6]Cl_2$ (**2**), $Mn(CH_3COO)_2 \cdot 4H_2O$ (**3**), $Mn(acac)_3$ (**4**), $Mn(SALADHP)_2$ (**5**), $[Mn(SALPN)O]_2$ (**6**), and $Mn(sal)_2(bipy)$ (**7**), where acac = acetylacetonate, Im = imidazole, SALADHP = dianion of 2-methyl-2-(salicylideneamino)-1,3-dihydroxypropan, SALPN = dianion of 1,3-bis(salicylideneamino)propan, sal = dianion of salicylic acid, and bipy = 2,2′-bipyridine. Hydrogen atoms in $Mn(SALADHP)_2$, $[Mn(SALPN)O]_2$, and $Mn(sal)_2(bipy)$ were added automatically using ArgusLab software,[78] with bond lengths of 0.95, 0.96, and 0.95 Å, respectively, from the heavy atoms. Unlike the other compounds, which all exist in crystal networks as separate units, the $[Mn_2(CH_3COO)_7 \cdot 3H_2O]^{3-}$ moiety is part of an infinite one-dimensional chain[73] in the crystal. Although the structural unit used in the computations retained all of the ligands surrounding two inequivalent Mn atoms plus one additional water molecule, it might not necessarily represent the most stable structure. As a consequence, some of the oxygen ligands that are normally coordinated to neighboring Mn atoms in the crystal network were left uncoordinated in the calculated structure, leading to the negative charge of 3− on the cluster.

The geometries of all complexes except $[Mn_2(CH_3COO)_7 \cdot 3H_2O]^{3-}$ were fully optimized with the ADF package[79] using the local density approximation of Vosko, Wilk, and Nusair[80] (VWN), the exchange gradient correction proposed by Becke[81] (B), and the correlation term of Perdew[82] (P86) combined with the all-electron Slater-type basis set of triple-ζ plus polarization (TZP) quality.[83] No symmetry constrains were set during geometry optimizations. Calculations were performed within the unrestricted scalar ZORA relativistic formalism.[84] Only the high-spin states of the complexes were evaluated, based on the experimental data.[75,77,85−87] Compounds containing two Mn atoms were calculated as the ferromagnetic configuration.

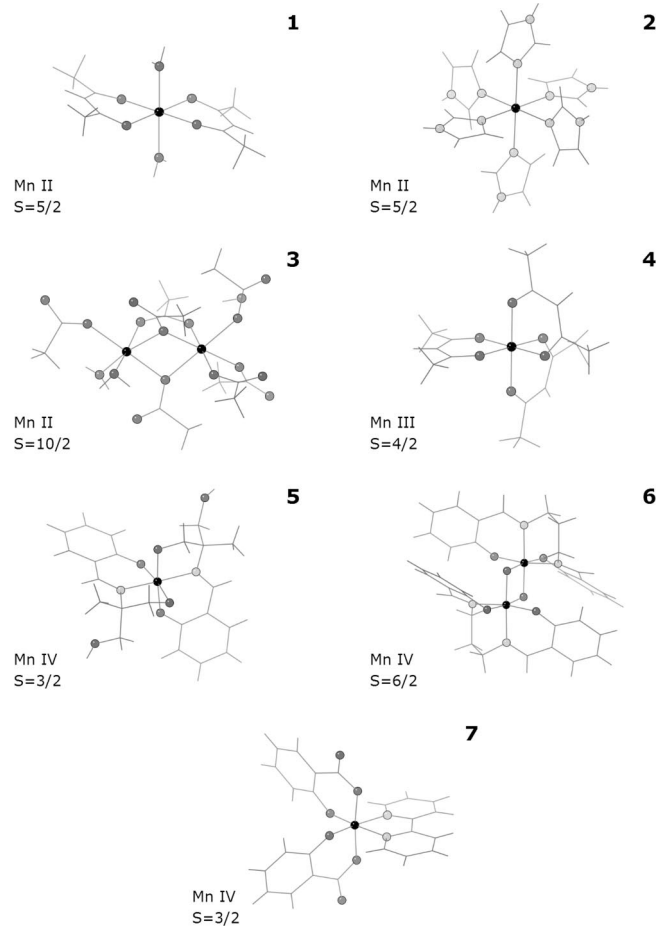

Figure 1. Structures of the Mn complexes studied. Manganese atoms are indicated by black balls, oxygen atoms by dark gray balls, and nitrogen atoms by light gray balls.

TDDFT calculations were performed at the BP86/TZP level using ADF. For comparison, the LB94 functional[88] was also evaluated by calculating core excitations for **1**, **2**, and **4**−**6**. In all TDDFT calculations, the adiabatic local density approximation was employed for the XC kernel,[89] and only spin-allowed excitations were considered. To evaluate the effect of the basis set, core excitations for **1** were also calculated using an even-tempered basis set of quadruple-ζ plus three polarization plus two diffuse functions (ET-QZ3P-2diff) quality for Mn atoms together with a basis set of even-tempered quadruple-ζ plus three polarization functions (ET-QZ3P) quality[83] for oxygen atoms connected to the manganese and a TZP basis set for the rest of the molecule (the whole set described hereafter as QZ3P+D for simplicity).

Only the first 120−150 lowest-energy excitations to the orbitals above and within the HOMO [singly occupied molecular orbital (SOMO)] level were considered for Mn 2p electrons. The present implementation of TDDFT in the ADF package does not account for spin−orbit coupling effects for open-shell systems,[90,91] a term that is of importance in the description of L-edge excitations in transition metals.[62] In fact, spin−orbit coupling is responsible for the X-ray absorption spectrum of 2p core electrons excited from heavy elements showing two

manifolds of excited states, associated with the $2p_{3/2}$ (L_3) and $2p_{1/2}$ (L_2) spin−orbit-coupled core states. For transition metals, the L_2 and L_3 edges are additionally coupled with 3d electron states (multiple effects), which results in the very complex absorption line shapes of both edges, separated by ca. 11 eV in Mn compounds.[92] Although subject to limitations, the present computational approach is, however, the best possible using currently available techniques for calculating L-edge energies.

The energies of the Mn 1s core electron excitations to orbitals lying up to ca. 200 eV above the HOMO (SOMO) level were calculated. To make the calculations tractable, this large one-electron excited configuration space was divided into subspaces, allowing computations on 100−150 core excitations to be performed in one computational job.

Excitations from each individual Mn 2p and 1s orbital were calculated separately. All excitation energies were first sorted by the oscillator strength, f, and only data with $f > 10^{-4}$ au for 1s and $f > 10^{-3}$ au for 2p core excitations were included in the subsequent analysis. Because the experimental spectra are normally collected with an energy scan resolution of 0.1−0.3 eV in the K-edge region, the calculated excitations of high intensity positioned within 0.1−0.6 eV of one another were assumed to contribute to the intensity of one "main peak", with an intensity-weighted energy position. If there were several main peaks of the above type, with similarly high intensity, the position of the final main peak was obtained by averaging the positions of the main peaks, for many of the analyses used here. In some cases, preference was given to a smaller number of high-intensity transitions over a larger number of lower-intensity transitions spanning the same energy range. This was achieved by a comparison of the sum of squares rather than just the sum of predicted oscillator strengths corresponding to the transitions contributing to the intensity of one main peak, when choosing the number of main peaks with similar high intensity before the final averaging.

This simple methodology is justified when comparing the position of the main peaks to the edge positions determined using the half-high or integral methods of analyzing the experimental spectra, assuming that the calculated energies of the transitions with high intensity correspond to the major peak or the rising edge of the experimental spectra. Such a justification is not as apparent when comparing computational results with edge energies determined by the other commonly used technique, the first-inflection-point method, especially for systems exhibiting fine structure on the rising edge. Rather, this requires convolution of each particular transition with some line shape (e.g., Gaussian) function and double differentiation of the resulting total signal. However, the edge-energy values obtained in this way are influenced by unknown parameters, such as the full widths at half-maximum (fwhm) of the Gaussians applied to each transition. Because even the inflection-point method generally involves local data smoothing,[14] the simple averaging method is favored here for comparison with the experimental edge data. However, peak positions determined from Gaussian-convoluted excitations with oscillator strengths greater than 10^{-4} au were also examined (see section 3.4) and discussed in relation to the edge region of the X-ray absorption spectra. The positions of main peaks determined by any of these methods are not expected to be more precise than 0.1 eV.

3. Results and Discussion

The X-ray absorption spectra of 1s electrons in Mn compounds exhibit three main energy regions. The pre-edge region is characterized by low-intensity absorptions associated with transitions to the metal d levels (of quadrupole nature) in the lowest part and to the localized Mn 4p-type levels in the higher pre-edge part. The next region is also related to the electronic structure of the Mn atom and is characterized by an edge energy of ca. 6.5 keV, thought to be associated with excitations above the metal 3d levels to orbitals that involve an admixture of metal 4p character. It is ca. 10 eV wide, and together with the next region of ca. 40 eV exhibiting near edge X-ray absorption fine structure, it constitutes XANES. The EXAFS region, lying more than 50 eV from the absorption edge, corresponds to excitations into the continuum level, with a photoelectron having enough kinetic energy to move freely through the material. It is characterized by fine structure containing information about the local atomic/ligand environment of the manganese. In this article, we focus on the edge region of 1s X-ray absorption but also investigate the edge region of 2p X-ray absorption that originates from the excitations of Mn 2p electrons to the metal 3d levels.

3.1. Bis(acetylacetonato)manganese(II) Dihydrate. *K-Edge Energy.* Figure 2 and Table 1 present results of TDDFT BP86/TZP calculations performed for the Mn 1s electron excitations of **1**, with the geometry optimized at the BP86/TZP level of theory. Only transitions with oscillator strengths greater than 10^{-4} au are shown on the graphs. The striking feature is the presence of a very strong transition of a β electron from the 1a to 288a orbital at 6474.7 eV (see also Supporting Information), which is ca. 54 eV higher than the predicted position of the near forbidden transition to the lowest unoccupied molecular orbital (LUMO). The final state is strongly delocalized on the ligand atoms, with ca. 4% admixture of Mn p orbitals. The character of the final state suggests that the excitation can be regarded as a main edge transition. The strong intensity, compared to any other relevant transitions, identifies it as the main peak of the spectrum, and therefore, it is likely to have the largest effect on the position of the K-edge of the X-ray absorption spectrum of **1**. However, the absolute energy predicted by TDDFT is ca. 70 eV lower than the experimental value of 6546.0 eV, which was reported for the position of the first major inflection point on the rising edge.[93]

To test whether this low absolute value of the edge energy was the effect of the functional used, the same calculations were performed with the LB94 method (Figure 2). It has been argued[64,66] that this functional, which has an asymptotic behavior in the regions far from the nucleus, provides a better description of the virtual orbitals, especially those of Rydberg type lying above the valence level. The results of LB94/TZP calculations do indeed show a significant improvement of ca. 60 eV in the computed transition energy, with the main peak at 6536.0 eV, which is within 10 eV of the experimental K-edge energy. However, the overall pattern (Figure 2) of the predicted excitations remains practically the same. The strongest transition is that of a β electron from the 1a to the 288a orbital, and its energy is ca. 55 eV higher than that predicted for the forbidden transition to the LUMO. Again, the final state is strongly delocalized on the ligand atoms (see Supporting Information), with ca. 2% admixture of Mn p orbitals. It seems that the main effect of using the LB94 functional instead of BP86 to calculate Mn 1s core excitations is to shift the whole spectrum to higher energies, while leaving the characteristics of the spectrum largely unchanged.

Further, it appears that the main cause of this higher energy shift is a lowering of the 1s orbital energy itself, by ca. 67 eV, rather than any different description of the high-energy unoc-

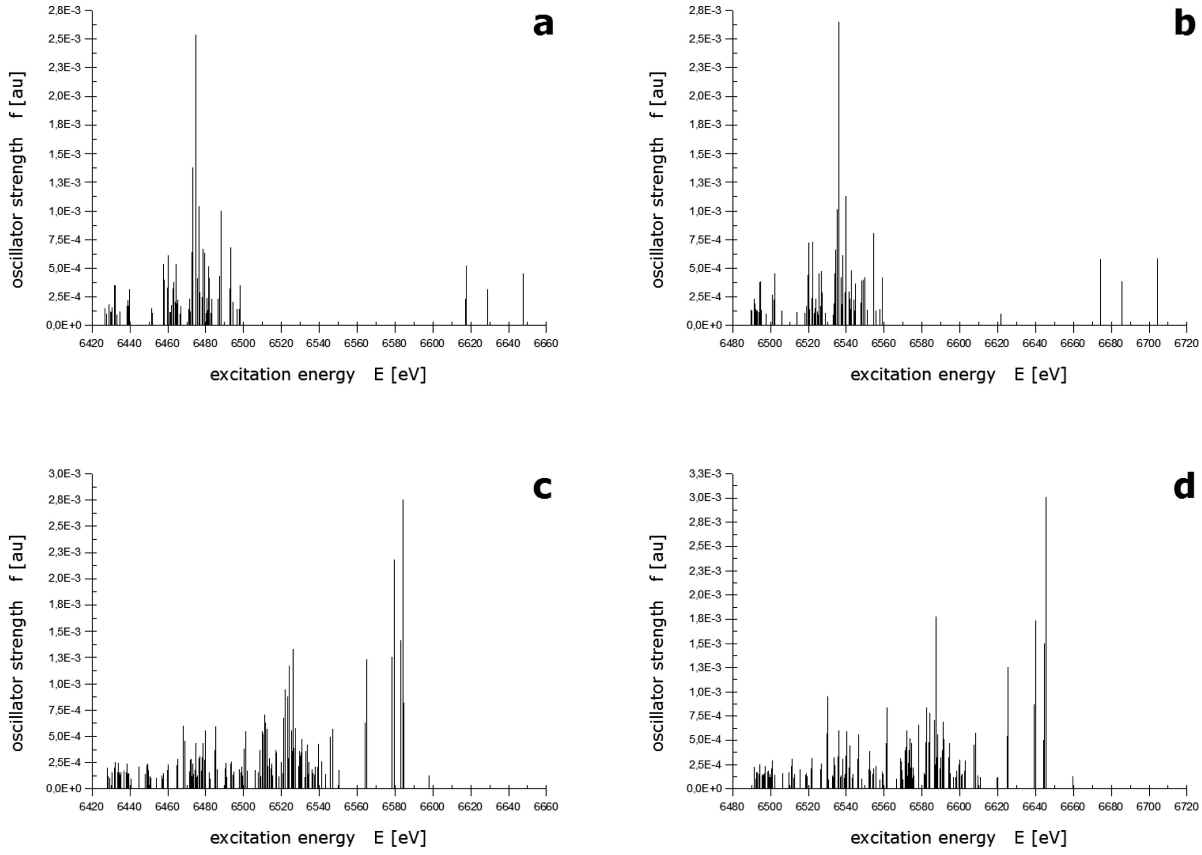

Figure 2. TDDFT excitation energies [E (eV)] and oscillator strengths [f (au)] for Mn 1s X-ray absorption spectra of $Mn(acac)_2 \cdot (H_2O)_2$ calculated at the (a) BP86/TZP, (b) LB94/TZP, (c) BP86/QZ3P+D, and (d) LB94/QZ3P+D levels with the BP86/TZP geometry. Only transitions with oscillator strengths greater than 10^{-4} au are shown.

TABLE 1: TDDFT Excitation Energies [E (eV)] and Oscillator Strengths [f (au)] for Mn 1s X-ray Absorption Spectra of Different Mn Complexes Calculated at the BP86/TZP Level with BP86/TZP Geometries

E	$f \times 10^3$	initial → final state[a]	E	$f \times 10^3$	initial → final state[a]
$Mn(acac)_2 \cdot (H_2O)_2$[b]			Mn(SALADHP)$_2$[c]		
6474.69	2.55	1a → 288a β	6488.86	0.49	1a → 522a + 523a β
$[Mn(Im)_6]^{2+}$[d]			6488.92	0.75	1a → 523a + 522a β
6479.37	1.35	1a → 481a β	6489.04	0.37	1a → 524a β
6479.52	1.62	1a → 482a β	[Mn(SALPN)O]$_2$[e]		
6479.52	1.63	1a → 483a β	6487.91	0.50	2a → 748a α
$Mn(acac)_3$[f]			6488.05	0.63	1a → 747a β
6486.83	0.32	1a → 390a + 389a β	6488.22	0.77	2a → 748a β
6486.84	0.69	1a → 389a + 390a β	6488.42	0.66	1a → 749a β
6486.95	0.35	1a → 391a β			
6487.10	0.72	1a → 392a β	6489.28	0.50	1a → 753a β
6487.23	0.38	1a → 393a β	6489.45	0.45	1a → 755a α
			6489.78	0.84	1a → 755a β
6488.12	1.02	1a → 395a β			

[a] Only selected transitions consisting of main peaks are shown; for mixed configurations, a contribution from a particular state is included in the description only if greater than 10%. Subsequent p-orbital character values rounded up to nearest 1%. [b] 288a: 4% Mn p. [c] 522a: <1% Mn p. 523a: 3% Mn p. 524a: 1% Mn p. [d] 481a: 10% Mn p. 482a: 13% Mn p. 483a: 13% Mn p. [e] 747a: 3% Mn p. 748a: 3% Mn p. 749a: 6% Mn p α, 10% Mn p β. 753a: 7% Mn p. 755a: 3% Mn p α, <1% Mn p β. [f] 389a: 3% Mn p. 390a: 4% Mn p. 391a: 13% Mn p. 392a: 6% Mn p. 393a: 6% Mn p. 395a: 20% Mn p.

cupied orbitals by the LB94 functional. By comparison of the Kohn−Sham (KS) orbital energies derived from the LB94 calculations, −6490.4 eV for 1a and 44.8 eV for 288a, one obtains a transition energy of 6535.3 eV that is only 0.7 eV less than that predicted by TDDFT. On the other hand, KS orbital energies of −6423.0 and 51.6 eV obtained using the BP86 functional result in a 1a → 288a electron transition value of 6474.6 eV, which is almost the same as predicted by TDDFT. To further investigate the functional dependence of the absolute transition energies, TDDFT calculations with the statistical averaging of (model) orbital potentials (SAOP) were performed. The strongest transition was predicted for an α electron excited from the 1a to the 288a orbital at 6473.8 eV, which is exactly equal to the difference in energy of the appropriate KS orbitals, −6427.7 and 46.0 eV, respectively. Thus, the SAOP approach developed to overcome shortcomings of the LB94 functional in the bonding region[94,95] shows underestimation of the absolute excitation energy similar to that seen with the BP86 functional. Again, the cause is mainly an insufficiently low energy of the 1s KS orbital. Similar behavior of the BP86 functional was reported previously.[96] An energy shift of 61.22 eV was determined as the necessary correction with this functional when excitations of 1s electrons of sulfur were compared with experimental values. Because the present work is concerned mainly with relative excitation energies exhibited by different oxidation states and ligand environments of Mn, any essentially constant energy offset is of reduced importance and is absorbed within the correlations that are established.

When excitations to higher levels are considered, especially excitations to the Rydberg excited states, larger basis sets with

additional polarization functions, augmented with diffuse functions, are recommended[62,64,97] for atoms, ions, or small molecules. Such an enlargement, for example, the ET-QZ4P-2diff basis set in the case of atoms and di- and triatomic molecules,[64,97] is usually not necessary for larger systems, where even the DZP basis set is often a good compromise between accuracy and computational effort.[63] However, to test the possibility of further improvement in the prediction of the absolute value of the edge energy, we performed additional calculations with extended basis sets on Mn (ET-QZ3P+2diff) and oxygen atoms (ET-QZ3P) connected to the metal atom, in accordance with the general assumption that core excitations are localized on a specific atomic site and, therefore, a better theoretical description of this region should lead to an improvement in the predicted transition energies.

Unexpectedly, increasing the basis set size dramatically changes the whole pattern of the excitations (Figure 2; see also Supporting Information). Although the LB94 and BP86 results are still consistent with each other, the outcomes are quite different from those obtained using the TZP basis set. The transition of strongest intensity is now predicted at 6584.3 eV by BP86 and at 6645.4 eV by LB94, which are ca. 38 and 99 eV, respectively, above the K-edge position determined experimentally.[93] Assuming that this calculated excitation corresponds to the experimentally observed value of the edge energy, it would appear that increasing the size of the basis set results in the energy predictions deteriorating by up to 100 eV. Analysis of the final state shows that it is highly localized on the atoms directly connected to Mn and on the metal atom itself, with 25% and 40% Mn p-type character based on the BP86 and LB94 results, respectively. This erratic behavior could be attributed to numerical instabilities, caused by linear dependency, due to strong overlap of the very diffuse functions on the Mn with the off-center functions from the larger basis sets on the oxygen atoms. Based on studies of the core excitations in MgO clusters, it has been suggested that basis sets beyond TZP should be avoided to prevent such instabilities.[63]

L-Edge Energy. In addition to the Mn 1s excitations, a series of calculations was performed to simulate the excitations of Mn 2p core electrons and to evaluate the effects of the functional and basis set used in these calculations. In contrast to the case for 1s excitations, there is no significant difference between results obtained using TZP and QZ3P+D basis sets (see Supporting Information). This is understandable, because only the 150 lowest-energy transitions were considered, so increasing the basis set should not affect the description of the molecular orbitals and therefore the excitations in this energy range. On the other hand, slight differences are observed between BP86 and LB94 results, but in this energy range, the advantage of the asymptotic functional over BP86 is not obvious. The position of the most intense peak is calculated at 624.7 eV using BP86/TZP, 640.0 eV using LB94/TZP, 624.5 eV using BP86/QZ3P+D, and 639.6 eV using LB94/QZ3P+D, all of which involve the excitation of the 2p β electron to a state with predominantly 3d character (see Supporting Information). The energy shift toward higher values when the LB94 functional is used can again be attributed mainly to a decrease in energy of the 2p orbital itself (by ca. 21 eV for the corresponding LB94 and BP86 orbitals) and, therefore, not to a different description of the energy of the final state.

Geometry Considerations. Different functionals and basis sets were also used to calculate excitation energies for the structure based on the XRD geometry. The same general difference between the results obtained with TZP and QZP3P+D for 1s excitations was observed. Similarly, slightly different patterns of excitations from 2p orbitals were predicted by the BP86 and LB94 functionals (see Supporting Information).

TABLE 2: Positions of the Main Peaks (eV) in the Mn 1s and 2p X-ray Absorption Spectra of Different Mn Complexes Calculated by TDDFT at the BP86/TZP Level with Different Geometries

parameter	ADF geometry	XRD geometry
	$Mn(acac)_2 \cdot (H_2O)_2$	
Mn−O (acac) (Å)	2.11	2.13
Mn−O (H_2O) (Å)	2.43	2.26
ρ_{spin} (Mn) (e)	4.80	4.80
$\hat{S}^2$	8.76	8.76
1s excitations	6474.7	6477.4
2p excitations	624.8	624.6
	$[Mn(Im)_6]^{2+}$	
Mn−N (Å)	2.29	2.28
ρ_{spin} (Mn) (e)	4.93	4.94
$\hat{S}^2$	8.76	8.76
1s excitations	6479.5	6480.3, 6481.5
2p excitations	625.5	625.7
	$Mn(acac)_3$	
Mn−O_{axial} (Å)	2.18	1.95
Mn−O_{planar} (Å)	1.94	2.00
ρ_{spin} (Mn) (e)	3.86	3.85
$\hat{S}^2$	6.05	6.05
1s excitations	6487.0, 6488.1	6485.7
2p excitations	627.3	627.6
	$Mn(SALADHP)_2$	
Mn−O (Å)	1.90	1.90
Mn−N (Å)	2.00	2.00
ρ_{spin} (Mn) (e)	2.70	2.71
$\hat{S}^2$	3.79	3.79
1s excitations	6488.9	6487.6, 6489.8
2p excitations	628.4	628.0
	$[Mn(SALPN)O]_2$	
Mn−O (Å)	1.94	1.92
Mn−$O_{bridged}$ (Å)	1.83	1.81
Mn−N (Å)	2.05	2.03
ρ_{spin} (Mn) (e)	2.73	2.72
$\hat{S}^2$	12.07	12.07
1s excitations	6488.2, 6489.7	6489.2, 6490.4, 6492.8
2p excitations	628.2	628.1

The most important difference between the BP86/TZP results obtained for the XRD and optimized structures is a distinct shift in the position of the main peak corresponding to the 1s transitions predicted for the XRD structure compared to the optimized geometry, while the 2p excitation energies are almost unaffected (Table 2). This shift of ca. 2.7 eV to higher energy for the 1s excitations is associated with significantly shorter Mn−O distances for the water molecules in the XRD structure compared to the computationally optimized values.

In the following sections, the results of TDDFT calculations are discussed mainly in relation to the BP86/TZP-optimized structures. However, because the complexes mostly involve large chelating ligands, the computed structures are typically very similar to the XRD geometries. When a basis set of TZP quality is applied to the whole molecule, the optimized structures provide an excellent description of the hydrogen atoms, the positions of which are not satisfactorily determined in the XRD structures. The calculations for **3** were only performed using a geometry based on the reported XRD structure.

3.2. Manganese K-Edge XAS. The patterns of 1s excitations predicted for **2** and **4**−**6** by BP86/TZP calculations on the optimized geometries are shown in Figure 3. They are all characterized by a concentration of high-intensity transitions

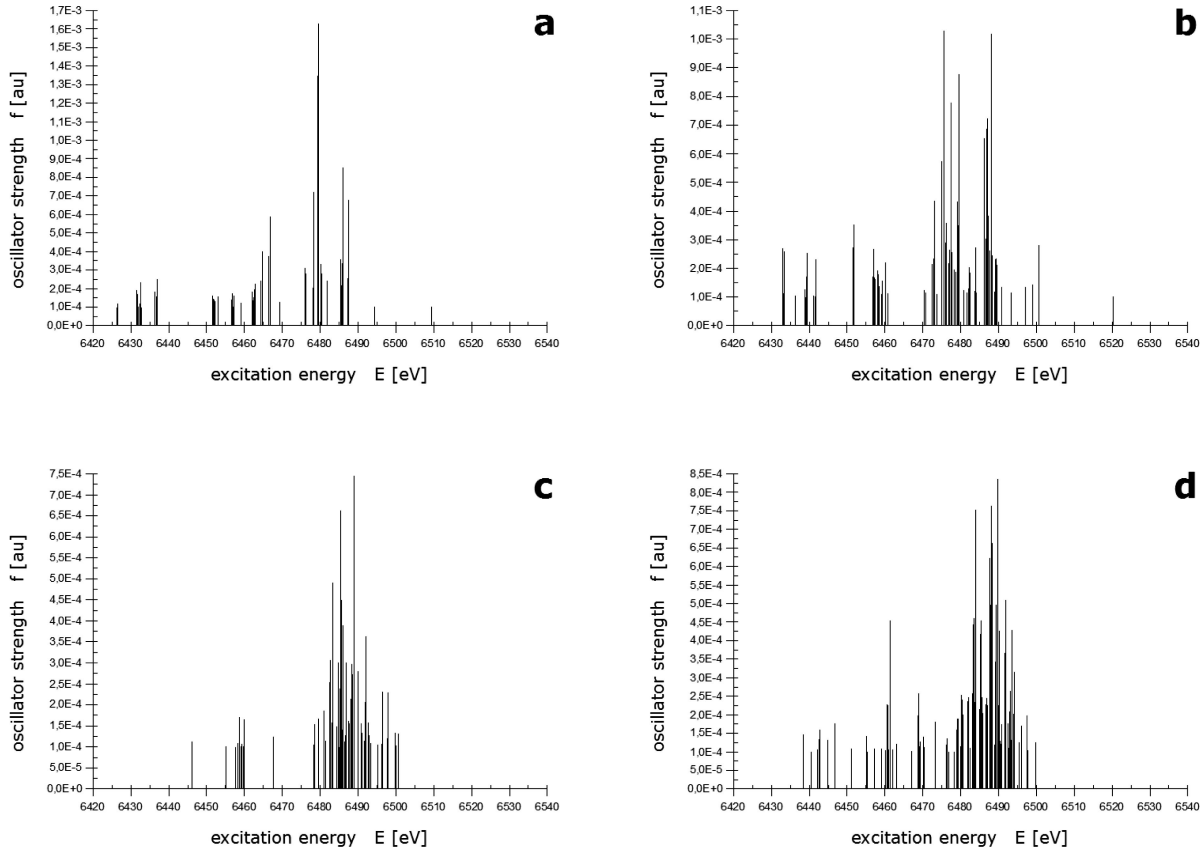

Figure 3. TDDFT excitation energies [E (eV)] and oscillator strengths [f (au)] for Mn 1s X-ray absorption spectra of (a) $[Mn(Im)_6]^{2+}$, (b) $Mn(acac)_3$, (c) $Mn(SALADHP)_2$, and (d) $[Mn(SALPN)O]_2$ calculated at the BP86/TZP level with BP86/TZP geometries. Only transitions with oscillator strengths greater than 10^{-4} au are shown.

within a 10−15 eV energy range and can be analyzed in a similar fashion to **1**.

Table 1 contains selected transitions for different complexes from the BP86/TZP computations, which are important to visualize the complex structure of the main peaks. It illustrates the most important components associated with the 1s electron transitions to the states with some Mn p-orbital character. TDDFT results predict one main peak for **2** localized at 6479.5 eV; two main peaks at 6487.0 and 6488.1 eV for **4** with an average position at 6487.6 eV; one main peak at 6488.9 eV for **5**; and two main peaks at 6488.2 eV and 6489.7 eV for **6**, averaging to 6489.0 eV. The predicted values exhibit a strong dependence on the oxidation state of the Mn, corresponding to ca. 10 eV change for the edge-energy position on going from the 2+ to 4+ state, with a more pronounced shift for the 2+ to 3+ than for the 3+ to 4+ one-electron advancements. The same general trend is predicted by BP86/TZP computations performed on the XRD geometries. However, differences are observed in the number and positions of the main peaks (Table 2; see also Supporting Information).

The positions of all main peaks predicted for the different geometries of the Mn complexes are shown in Figure 4, where they are plotted against K-edge energy positions determined experimentally[30] by the first-inflection-point method. A reasonably good correlation is observed for the XRD structures (Figure 4a), which improves significantly for the energies determined by the BP86/TZP method based on the optimized structures (Figure 4b).

Figure 4a also contains main peaks determined by the BP86/TZP method for the XRD geometry of **3**, plotted against the corresponding experimental edge energy of 6548.6 eV.[30] This complex was included in the calculations even though it was not possible to optimize its geometry due to the extended nature of the structure. Surprisingly, even if the positions of two main peaks predicted for **3** at 6479.4 and 6480.1 eV, averaging to 6479.6 eV, are lower than expected by comparison with the predicted values for **2** and the experimentally determined difference of the edge energy between **2** and **3**, they still fit reasonably within the range of positions expected for Mn(II) complexes. Thus, the edge energies obtained for **3** from TDDFT calculations are quite satisfactory, suggesting that only minor changes in the model geometry would be required to obtain closer correlation with the experimental data.

Better correlation between the predicted and experimentally determined K-edge energies occurs with the BP86 rather than the LB94/TZP results. The latter (Figure 4c) show one main peak localized at 6541.4 eV for **2**; one main peak at 6547.9 eV for **4**; one main peak at 6546.4 eV for **5**; and three main peaks at 6543.2 eV, 6548.8, and 6550.7 eV for **6**, averaging to 6547.6 eV. Although these values are much closer in overall magnitude to the experimental data, as observed for **1** above, the detailed trend between the oxidation state of the Mn and the position of the edge energy, as observed for the BP86 results, is not maintained. Even the qualitative ranking of transition energy with oxidation state is lost.

Figure 5 summarizes BP86/TZP results obtained for different Mn complexes, including the edge energy of **1** predicted on the basis of its XRD geometry and plotted against the available experimental data.[93,98] Good correlation with the experimentally determined values is clearly visible, especially for the optimized geometries. However, when DFT optimization for a particular system is not feasible, then the XRD structures can still be

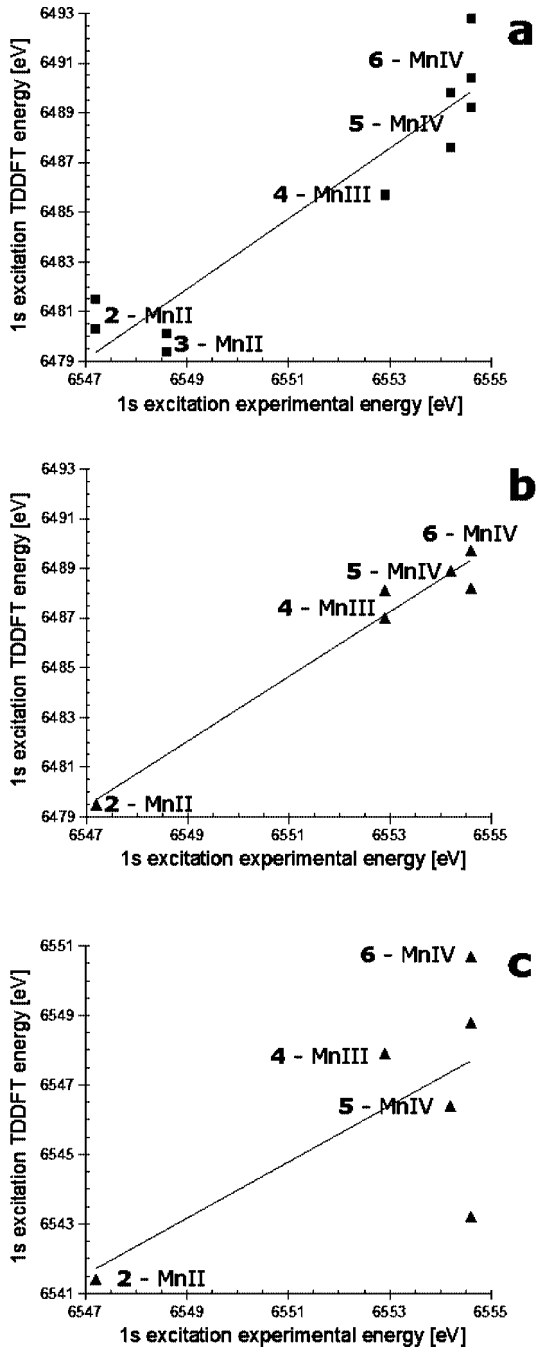

Figure 4. Relation between experimental and TDDFT excitation energies (eV) for Mn 1s X-ray absorption spectra of different Mn complexes calculated at the BP86/TZP level with (a) XRD and (b) ADF geometries and (c) at the LB94/TZP level with ADF geometries.

usefully employed. Furthermore, regions of the plot corresponding to complexes with Mn in the 2+, 3+, and 4+ oxidation states are clearly distinguishable. The BP86/TZP results agree with the experimental observation[30] that a larger shift of K-edge energy is seen between Mn(II) and Mn(III) than between Mn(III) and Mn(IV). Averaging all of the results presented in Figure 5 for different complexes containing Mn atoms at the same formal oxidation state, one obtains values of 5.6 and 7.2 eV for the K-edge energy differences of Mn(II) and Mn(III) from experiment and theory, respectively, and corresponding differences of 1.5 and 2.7 eV for Mn(III) and Mn(IV). This conclusion is significant for determining the Mn oxidation levels in the S states of PSII and suggests that the $S_0 \rightarrow S_1$ transition, characterized

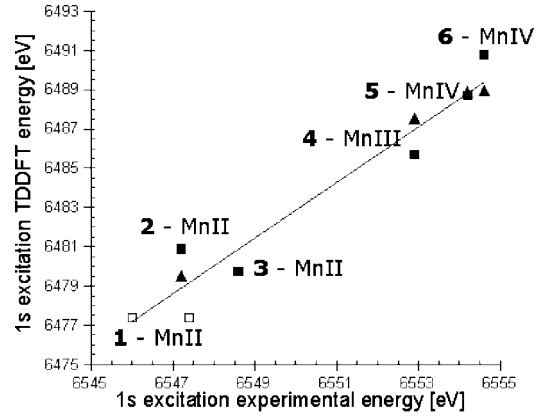

Figure 5. Relation between experimental and TDDFT excitation energies (eV) for Mn 1s X-ray absorption spectra of different Mn complexes calculated at the BP86/TZP level with (■) XRD and (▲) ADF geometries. Only average main-peak positions from Figure 3a,b are shown. Additional points for **1**, based on BP86/TZP calculations with the XRD geometry, are included (□).

by the largest K-edge energy shift observed experimentally during $S_0 \rightarrow S_3$ advancement,[8] is most probably a Mn(II) → Mn(III) oxidation.

The LB94 functional does not reproduce the experimentally observed correlation between the K-edge energy and the oxidation state of the Mn ions, and a detailed analysis suggests that this might be related to the calculated spin densities of the systems. The LB94 functional gives total spin populations on Mn atoms of 4.74, 3.64, 2.47, and 2.53 e for **2** and **4**−**6**, respectively. These values are significantly lower than those obtained from the BP86 calculations (4.93, 3.86, 2.70, and 2.73 e, respectively), and the differences are greatest for the Mn(IV) complexes, where the LB94 results show more than 0.5 e difference from the formal number of three d electrons expected for Mn in this case. Assuming that the BP86 description of the metal d orbitals is more realistic, the difference between the total spin population on the Mn predicted by LB94 and BP86 functionals divided by the formal number of d electrons is a measure of the underestimation of d-type spin population on the Mn by the LB94 functional. These differences for **2** and **4**−**6** plotted against the corresponding difference in the excitation energy predicted by the LB94 and BP86 functionals show an almost linear correlation (see Supporting Information). The favorable shifting of the 1s excitation energies toward higher values, observed for the LB94 functional in comparison with the BP86 functional, is smaller for those structures in which the total spin properties of the ground state are less well described by the LB94 functional (see Supporting Information). In other words, the inadequate description of the ground state by the LB94 functional is associated with the less accurate prediction of excitation energies from that state. The poorer description of the ground-state spin properties of the systems provided by the LB94 functional can be readily rationalized on the basis that the functional was constructed mainly to show good asymptotic behavior at large distances from the nucleus, but at the cost of a poorer description of regions closer to the nucleus. In principle, a more accurate description of the levels far above the occupied orbitals should improve the predictions of electron transitions to these levels. However, even if the LB94 functional behaves better than the Becke exchange functional for core and Rydberg regions, the opposite is true for the valence regions. The deficiencies of the LB94 functional in the inner-molecular/bonding areas result mainly in an inadequate description of the low-energy excitation

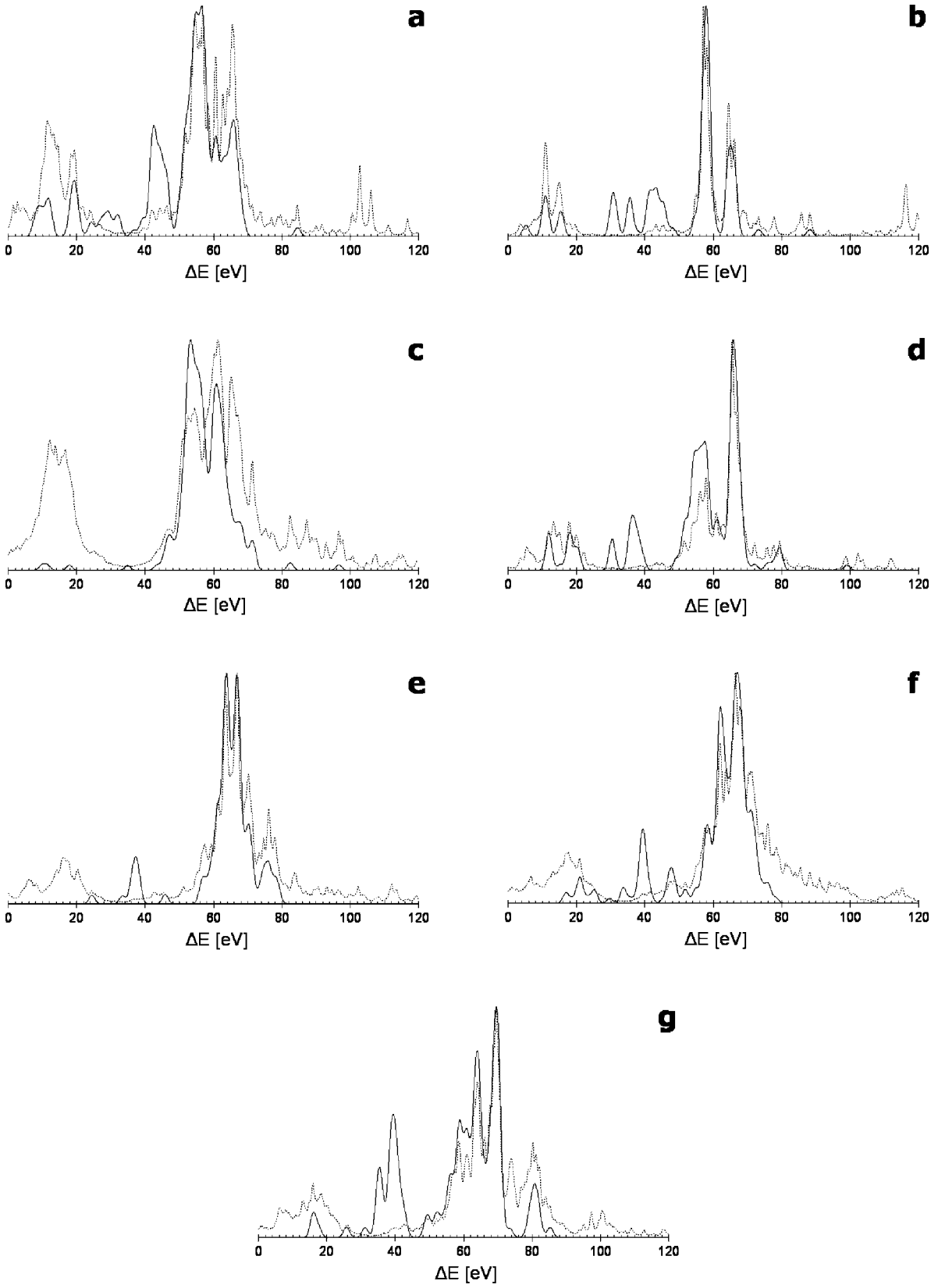

Figure 6. Mn p PDOS profiles (dashed line) vs Mn 1s excitation profiles (solid line) for (a) **1**, (b) **2**, (c) **3**, (d) **4**, (e) **5**, (f) **6**, and (g) **7**. The peaks in the PDOS curves are convoluted with Lorentzian functions (fwhm = 0.5 eV), and excitation profiles were obtained by Gaussian convolution (fwhm = 2.5 eV) of the excitations with oscillator strengths greater than 10^{-4} au. Energies are referenced to the energy level of the lowest unoccupied molecular orbital and to the excitation of a Mn 1s electron to this orbital. Partial density of states is projected on the p-type symmetrized fragment orbital characterized by the orbital energy of 206.91 eV in the free Mn atom, based on the BP86/TZP calculations.

energies in the visible and near-UV regions.[94,95] The above results suggest that, at least for some open-shell systems, a deficient description of the valence levels can also be an important factor in the prediction of the core excitations. This prevents the LB94 functional from being useful in a detailed quantitative analysis of the type performed here. This is

TABLE 3: Ionization Energies, Orbital Energies of the LUMO, and Excitation Energies from the Mn 1s Orbital to the LUMO Calculated at the BP86/TZP Level

complex	geometry	total charge	E_{LUMO}[a] (eV)	$E_{excitation}$[b] (eV)	E_{ion}[c] (eV)
1	XRD	0	−1.90	6420.54	6595.04
2	ADF	2+	−7.05	6421.26	6600.98
3	XRD	3−	5.46	6419.31	6585.58
4	ADF	0	−3.03	6421.28	6595.49
5	ADF	0	−3.39	6421.80	6595.67
6	ADF	0	−3.24	6421.61	6595.33
7	ADF	0	−4.06	6421.63	6596.17

[a] Energy of the lowest unoccupied molecular orbital. [b] For the transition of a 1s electron of a manganese atom to the lowest unoccupied molecular orbital. [c] Average value of the difference between the total energy calculated for the XRD geometry of a complex and the total energy of the same system with an α-spin or β-spin electron removed from the 1s orbital of manganese.

especially true because the extent of the erratic spin description exhibited by the LB94 functional cannot be reasonably predicted a priori for each molecule. To overcome the shortcomings of the LB94 functional in the bonding region and to take advantage of its good behavior in the core and Rydberg regions, a meta-GGA functional was recently proposed[99] that combines the Lee−Yang−Parr (LYP) correlation functional with the Becke 88 (B88) exchange functional in the valence region and the LB94 functional in the core and asymptotic regions. However, meta-GGA functionals are still unavailable for TDDFT calculations in the ADF package, and therefore, they could not be tested at this time.

3.3. Manganese L-Edge XAS. Based on results of BP86/TZP calculations performed on the optimized geometries, high-intensity excitations of 2p electrons are located within a range of ca. 3 eV for **2**, **4**, and **5** and ca. 4 eV for **6** (see Supporting Information). Analyzing the results allows one to localize only one main peak of high intensity for each structure, positioned at 625.5 eV for **2**, 627.3 eV for **4**, 628.4 eV for **5**, and 628.2 eV for **6**. Thus, the BP86/TZP results suggest that a manganese oxidation state change from 2+ to 4+ increases the excitation energy of the metal 2p electrons by ca. 3 eV. Even though the experimental data for the L-edge transitions of Mn complexes in different oxidation states are limited, TDDFT calculations were performed to test whether the general trend observed experimentally for manganese oxides is reproduced. The data show that, on going from $Mn^{II}O$ to $Mn^{IV}O_2$, the excitation energy, as evidenced by the position of the highest-intensity peak in the L_3 manifold,[92] increases by slightly more than 3 eV, from ca. 641.6 to 645.0 eV. This agreement between theory and experimental data is even more remarkable given the shortcomings of the present implementation of the TDDFT code in the ADF package, which does not account for spin−orbit coupling effects in open-shell systems.

A direct comparison of the theoretically predicted and experimentally determined energies of 2p excitations can be performed for **1**, **2**, and **7**. The BP86/TZP method gives one main peak at 627.8 eV when applied to the optimized structure of **7** (see Supporting Information), and the results of TDDFT calculations for **1** and **4** have already been described. Based on the 1s2p RIXS studies of these complexes,[33] the value of energy transfer, directly related to the L-edge energy, increases from 639.9 to 641.2 eV on going from Mn(II) of **1** to Mn(III) of **4** and then to 642.7 eV on going to Mn(IV) of **7**. Thus, from Mn(II) to Mn(IV), the values associated with L-edge energies shift by ca. 2.8 and 3.1 eV based on experimental and TDDFT results, respectively. Although the correlation between computational and experimental data is imperfect (see Supporting Information), the relation between the 2p excitation energy and the Mn oxidation state in the series of complexes is generally maintained.

3.4. Manganese XAS Edge Region. The pre-edge and edge regions of Mn K X-ray absorption spectra, although resulting from transitions of different intensity and involving different orbitals,[11] are both sensitive to the Mn oxidation state. The main peaks derived from TDDFT calculations, even if shifted in absolute value well below the Mn K pre-edge region when using the BP86 instead of the LB94 functional, clearly correspond to the edge and not pre-edge region of XAS. This is evident from the character of the predicted transitions, as well as the magnitude of the energy change on oxidation of the Mn.

The manganese p-type character of the excited orbitals involved in particular 1s electron transitions contributing to the main peaks (see Supporting Information) clearly indicates their edge and not pre-edge origin. This is clearly visualized in Figure 6, where the Mn 1s Gaussian-convoluted excitation profiles are plotted against the Mn p-orbital partial density of states (PDOS) profiles. The energies of the PDOS profiles are referenced to the energy level of the LUMO, whereas the Mn 1s excitation profiles are referenced to the energy of the Mn 1s-to-LUMO transitions (Table 3). It is evident for all complexes studied that the main peaks of the excitation spectrum overlap with the regions of highest density of one-electron states exhibiting Mn p-type character. (The partial density of states on the graphs is projected on the p-type symmetrized fragment orbital characterized by the orbital energy of 206.91 eV in the free Mn atom, based on the BP86/TZP calculations.)

Furthermore, as evidenced by the 1s2p RIXS studies on Mn complexes,[33] the incident energy, corresponding to the K pre-edge absorption energy, increases by ca. 0.8 eV on going from Mn(II) to **1** to Mn(III) of **4**, and then by another ca. 0.7 eV on going to Mn(IV) of **7**. On the other hand, the BP86/TZP method gives one main peak at 6491.4 eV when applied to the optimized structure of **7** (see Supporting Information) and localizes the main peak at 6474.7 and 6487.6 eV for **1** and **4**, respectively. The experimental pre-edge K energy shifts by ca. 1.5 eV on going from Mn(II) to Mn(IV), whereas TDDFT results show a significantly larger shift in the main peak positions (16.7 eV), in line with the much larger changes expected for the edge compared to pre-edge energies.[57] In fact, the difference between edge energies predicted by TDDFT for **1** and **4** (12.9 eV for optimized geometries) is quite close to the shift of 13.2 eV for the K-edge peak maximum for these complexes.[32] This suggests that the main peaks obtained from BP86/TZP studies can be identified directly with the principal absorption peaks on the top of the K-edge X-ray absorption spectra, before the onset of the EXAFS region. This is perhaps not surprising given the method of determining the positions of the main peaks and the averaging used here to analyze results from the TDDFT studies. However, when compared to the results obtained for the more reliable XRD geometry of **1**, the energy gap between **1** and **4** diminishes to 10.2 eV.

In a preliminary attempt to explore whether the predicted excitations contribute to the major peak or to the rising edge of the X-ray absorption spectrum, all excitations with oscillator strengths greater than 10^{-4} au were summed with Gaussian convolutions in order to determine the energies of the highest peaks (fwhm = 10 eV was used when analyzing results for all of the complexes except **4**, for which fwhm = 15 eV was used while determining the position of the highest peak based on

the TDDFT results obtained for the optimized geometry). A plot of these energies, analogous to Figure 5, displays a distinct correlation between the experimental and theoretical XAS edge energies, although not quite as good as Figure 5 (see Supporting Information). The main feature is an almost 1:1 correlation between the predicted values and the experimental edge-energy gap between Mn(II) of **2** and Mn(IV) of **6**, that is 7.6 eV based on the optimized geometries and 7.4 eV derived from experiment.

Because the present analysis is based solely on a one-parameter description of the experimental K-edge spectra and neglects factors such as the fine structure often seen on the rising edge, very specific interpretations are probably premature. Therefore, when referring to the edge energy in this article, in relation to TDDFT results and their correlation with experimental data, we do not differentiate between rising edge or major peak positions, as determined by XAS, but consider them both. Studies to computationally examine these matters in more detail are in progress, and they are further encouraged by promising results of a comparative analysis of TDDF calculations and the experimental K-edge metal X-ray absorption spectra reported recently for vanadium[66] and titanium[100] oxides.

4. Conclusions

In this article, we have presented TDDFT results for the 1s and 2p Mn core excitations of seven different manganese complexes with metal atoms in the 2+, 3+, and 4+ oxidation states. Our work shows that the BP86/TZP level of theory can successfully reproduce the experimentally observed correlation between the oxidation state of manganese and the Mn K-edge and L-edge energies, even if the absolute energy values predicted are significantly lower than the experimental data. Satisfactory results for 2p excitations are obtained even without the inclusion of spin−orbit coupling effects in the calculations. The Mn complexes examined contain a wide range of ligand types, but the experimental correlation between the oxidation state and the energies of 1s and 2p Mn excitations is reproduced, irrespective of the ligand environment. In particular, bonding and ligand effects are included in the calculations self-consistently, indicating the robustness of TDDFT in comparative analyses of XAS data.

The TZP basis set results in excitation patterns more consistent with experimental data than those obtained using the even-tempered QZ3P basis sets on both oxygen and manganese atoms with additional diffuse functions on the latter. For the systems studied, the LB94 functional produces basically the same 1s excitation patterns as BP86, but shifted to higher energies. This is mainly due to the lowering of core orbital energies by LB94 and not to a different description of the high-lying states. Additionally, in some cases, the LB94 functional leads to a poorer description of the valence region and the spin properties of the ground state, with a tendency to underestimate the population of d-type unpaired electrons in the system. This results in a failure to reproduce the experimentally observed correlation between the Mn oxidation state and the K-edge energy for the series of complexes studied.

The results of BP86/TZP calculations indicate that TDDFT can be successfully applied to explain the differences in the K-edge and L-edge energies between different transition metal complexes. Further calculations on different manganese systems are needed to clearly identify those transitions contributing to the major peak as opposed to the rising edge of the X-ray absorption spectra. Fine reproduction of the shape of the edge region based on TDDFT-predicted excitations should allow the same methodology to be applied in studies of important biocatalytic systems, including model Mn_4Ca clusters responsible for water oxidation in PSII.

Acknowledgment. The authors gratefully acknowledge financial assistance from the Australian Research Council. A.R.J. thanks the Faculty of Chemistry, University of Wroclaw, Wroclaw, Poland, for a two-year sabbatical to work as a postdoctoral fellow at the Australian National University. The computations were performed using the platforms of the Australian Partnership for Advanced Computing, operating through the Australian National University Supercomputer Facility, and of the Wroclaw Center of Networking and Supercomputing (Grant 48).

Supporting Information Available: ADF-optimized structures (XYZ) of Mn complexes and calculated TDDFT excitation energies for transitions with oscillator strengths greater than 10^{-4} au for 1s excitations and 10^{-3} au for 2p excitations. This information is available free of charge via the Internet at http://pubs.acs.org.

References and Notes

(1) Hill H. A. O.; Sadler P. J.; Thomson A. J. *Metal Sites in Proteins and Models*; Springer: New York, 1999.
(2) Stryer, L. *Biochemistry*; W. H. Freeman and Co.: New York, 2000.
(3) Albracht, S. P. J. *Biochim. Biophys. Acta* **1994**, *1188*, 167.
(4) Frey, M. *ChemBioChem* **2002**, *3*, 153.
(5) Burgdorf, T.; Löscher, S.; Liebisch, P.; Van der Linden, E.; Galander, M.; Lendzian, F.; Meyer-Klaucke, W.; Albracht, S. P. J.; Friedrich, B.; Dau, H.; Haumann, M. *J. Am. Chem. Soc.* **2005**, *127*, 576.
(6) Burgess, B. K.; Lowe, D. J. *Chem. Rev.* **1996**, *96*, 2983.
(7) Lovell, T.; Li, J.; Liu, T.; Case, D. A.; Noodleman, L. *J. Am. Chem. Soc.* **2001**, *123*, 12392.
(8) Åhrling, K. A.; Pace, R. J.; Evans, M. C. W. The catalytic manganese cluster: Implications from spectroscopy. In *Photosystem II: The Light-Driven Water:Plastoquinone Oxidoreductase*; Wydrzynski, T. J., Satoh, K., Eds.; Advances in Photosynthesis and Respiration Series; Springer: Dordrecht, The Netherlands, 2005; Vol. 22, p 285.
(9) McEvoy, J. P.; Brudvig, G. W. *Chem. Rev.* **2006**, *106*, 4455.
(10) Yano, J.; Yachandra, V. K. *Photosynth. Res.* **2007**, *92*, 289.
(11) de Groot, F. *Chem. Rev.* **2001**, *101*, 1779.
(12) Powers, L. *Biochim. Biophys. Acta* **1982**, *683*, 1.
(13) Hedman, B.; Frank, P.; Gheller, S. F.; Roe, A. L.; Newton, W. E.; Hodgson, K. O. *J. Am. Chem. Soc.* **1988**, *110*, 3798.
(14) Stemmler, T. L.; Sossong, T. M., Jr.; Goldstein, J. I.; Ash, D. E.; Elgren, T. E.; Kurtz, D. M., Jr.; Penner-Hahn, J. E. *Biochemistry* **1997**, *36*, 9847.
(15) Rehr, J. J.; Albers, R. C. *Rev. Mod. Phys.* **2000**, *72*, 621.
(16) Petrie, S.; Stranger, R.; Gatt, P.; Pace, R. J. *Chem. Eur. J.* **2007**, *13*, 5082.
(17) Kamiya, N.; Shen, J.-R. *Proc. Natl. Acad. Sci. U.S.A.* **2003**, *100*, 98.
(18) Ferreira, K. N.; Iverson, T. M.; Maghlaoui, K.; Barber, J.; Iwata, S. *Science* **2004**, *303*, 1831.
(19) Loll, B.; Kern, J.; Saenger, W.; Zouni, A.; Biesiadka, J. *Nature* **2005**, *438*, 1040.
(20) Roelofs, T. A.; Liang, W.; Latimer, M. J.; Cinco, R. M.; Rompel, A.; rews, J. C.; Sauer, K.; Yachandra, V. K.; Klein, M. P. *Proc. Natl. Acad. Sci. U.S.A.* **1996**, *93*, 3335.
(21) Ono, T.; Noguchi, T.; Inoue, Y.; Kusunoki, M.; Matsushita, T.; Oyanagi, H. *Science* **1992**, *258*, 1335.
(22) Haumann, M.; Müller, C.; Liebisch, P.; Iuzzolino, L.; Dittmer, J.; Grabolle, M.; Neisius, T.; Meyer-Klaucke, W.; Dau, H. *Biochemistry* **2005**, *44*, 1894.
(23) Kusunoki, M.; Ono, T.; Noguchi, T.; Inoue, Y.; Oyanagi, H. *Photosynth. Res.* **1993**, *38*, 331.
(24) Iuzzolino, L.; Dittmer, J.; Dörner, W.; Meyer-Klaucke, W.; Dau, H. *Biochemistry* **1998**, *37*, 17112.
(25) Sauer, K.; Yano, J.; Yachandra, V. K. *Photosynth. Res.* **2005**, *85*, 73.
(26) Dau, H.; Iuzzolino, L.; Dittmer, J. *Biochim. Biophys. Acta* **2001**, *1503*, 24.
(27) Messinger, J.; Robblee, J. H.; Bergmann, U.; Fernandez, C.; Glatzel, P.; Visser, H.; Cinco, R. M.; McFarlane, K. L.; Bellacchio, E.; Pizarro, S. A.; Cramer, S. P.; Sauer, K.; Klein, M. P.; Yachandra, V. K. *J. Am. Chem. Soc.* **2001**, *123*, 7804.
(28) Rao, B. J.; Chetal, A. R. *J. Phys. Chem. Solids* **1983**, *44*, 677.

(29) Belli, M.; Scafati, A.; Bianconi, A.; Mobilio, S.; Palladino, L.; Reale, A.; Burattini, E. *Solid State Commun.* **1980**, *35*, 355.
(30) Penner-Hahn, J. E.; Fronko, R. M.; Pecoraro, V. L.; Yocum, C. F.; Betts, S. D.; Bowlby, N. R. *J. Am. Chem. Soc.* **1990**, *112*, 2549.
(31) Visser, H.; Anxolabéhère-Mallart, E.; Bergmann, U.; Glatzel, P.; Robblee, J. H.; Cramer, S. P.; Girerd, J.-J.; Sauer, K.; Klein, M. P.; Yachandra, V. K. *J. Am. Chem. Soc.* **2001**, *123*, 7031.
(32) Glen, G. L.; Dodd, C. G. *J. Appl. Phys.* **1968**, *39*, 5372.
(33) Glatzel, P.; Bergmann, U.; Yano, J.; Visser, H.; Robblee, J. H.; Gu, W.; de Groot, F. M. F.; Christou, G.; Pecoraro, V. L.; Cramer, S. P.; Yachandra, V. K. *J. Am. Chem. Soc.* **2004**, *126*, 9946.
(34) Bader, R. F. W. *Atoms in Molecules. A Quantum Theory*; Clarendon Press: Oxford, U.K., 1990.
(35) Dau, H.; Liebisch, P.; Haumann, M. *Anal. Bioanal. Chem.* **2003**, *376*, 562.
(36) Weng, T.-C.; Waldo, G. S.; Penner-Hahn, J. E. *J. Synchrotron Radiat.* **2005**, *12*, 506.
(37) Wydrzynski, T. J., Satoh, S., Eds. *Photosystem II: The Light-Driven Water:Plastoquinone Oxidoreductase*; Advances in Photosynthesis and Respiration Series; Springer: Dordrecht, The Netherlands, 2005; Vol. 22.
(38) Carrell, T. G.; Tyryshkin, A. M.; Dismukes, G. C. *J. Biol. Inorg. Chem.* **2002**, *7*, 2.
(39) Kuzek, D.; Pace, R. J. *Biochim. Biophys. Acta* **2001**, *1503*, 123.
(40) Peloquin, J. M.; Britt, R. D. *Biochim. Biophys. Acta* **2001**, *1503*, 96.
(41) McDermott, A. E.; Yachandra, V. K.; Guiles, R. D.; Cole, J. L.; Dexheimer, S. L.; Britt, R. D.; Sauer, K.; Klein, M. P. *Biochemistry* **1988**, *27*, 4021.
(42) Messinger, J.; Nugent, J. H. A.; Evans, M. C. W. *Biochemistry* **1997**, *36*, 11055.
(43) Åhrling, K. A.; Peterson, S.; Styring, S. *Biochemistry* **1998**, *37*, 8115.
(44) Kulik, L. V.; Epel, B.; Lubitz, W.; Messinger, J. *J. Am. Chem. Soc.* **2005**, *127*, 2392.
(45) Britt, R. D.; Campbell, K. A.; Peloquin, J. M.; Gilchrist, M. L.; Aznar, C. P.; Dicus, M. M.; Robblee, J.; Messinger, J. *Biochim. Biophys. Acta* **2004**, *1655*, 158.
(46) Noguchi, T.; Ono, T.; Inoue, Y. *Biochim. Biophys. Acta* **1995**, *1228*, 189.
(47) Chu, H.-A.; Hillier, W.; Law, N. A.; Babcock, G. T. *Biochim. Biophys. Acta* **2001**, *1503*, 69.
(48) Jaszewski, A. R.; Siatecki, Z.; Jezierska, J. *Chem. Phys. Lett.* **2000**, *331*, 403.
(49) Jaszewski, A. R.; Jezierska, J. *Chem. Phys. Lett.* **2001**, *343*, 571.
(50) Neese, F. *Curr. Opin. Chem. Biol.* **2003**, *7*, 125.
(51) Neese, F. *J. Biol. Inorg. Chem.* **2006**, *11*, 702.
(52) Rehr, J. J. *Radiat. Phys. Chem.* **2006**, *75*, 1547.
(53) Ankudinov, A. L.; Ravel, B.; Rehr, J. J.; Conradson, S. D. *Phys. Rev. B* **1998**, *58*, 7565.
(54) Hatada, K.; Chaboy, J. *Phys. Rev. B* **2007**, *76*, 104411.
(55) Natoli, C. R.; Benfatto, M.; Longa, S. D.; Hatada, K. *J. Synchrotron Radiat.* **2003**, *10*, 26.
(56) Benfatto, M.; Longa, S. D. *J. Synchrotron Radiat.* **2001**, *8*, 1087.
(57) Nietubyć, R.; Sobczak, E.; Attenkofer, K. E. *J. Alloys Comp.* **2001**, *328*, 126.
(58) Modrow, H.; Bucher, S.; Rehr, J. J.; Ankudinov, A. L. *Phys. Rev. B* **2003**, *67*, 035123.
(59) Gilbert, B.; Frazer, B. H.; Belz, A.; Conrad, P. G.; Nealson, K. H.; Haskel, D.; Lang, J. C.; Srajer, G.; De Stasio, G. *J. Phys. Chem. A* **2003**, *107*, 2839.
(60) Chaboy, J.; Prieto, C.; Hernando, M.; Parras, M.; González-Calbet, J. *Phys. Rev. B* **2006**, *74*, 174433.
(61) Nalewajski, R. F., Ed. *Density Functional Theory*; Springer: Heidelberg, Germany, 1996.
(62) Fronzoni, G.; Stener, M.; Decleva, P.; Wang, F.; Ziegler, T.; van Lenthe, E.; Baerends, E. J. *Chem. Phys. Lett.* **2005**, *416*, 56.
(63) Stener, M.; Fronzoni, G.; De Francesco, R. *Chem. Phys.* **2005**, *309*, 49.
(64) Fronzoni, G.; De Francesco, R.; Stener, M.; Decleva, P. *J. Chem. Phys.* **2007**, *126*, 134308.
(65) Fronzoni, G.; Stener, M.; Reduce, A.; Decleva, P. *J. Phys. Chem. A* **2004**, *108*, 8467.
(66) De Francesco, R.; Stener, M.; Causà, M.; Toffoli, D.; Fronzoni, G. *Phys. Chem. Chem. Phys.* **2006**, *8*, 4300.
(67) Runge, E.; Gross, E. K. U. *Phys. Rev. Lett.* **1984**, *52*, 997.
(68) Bauernschmitt, R.; Ahlrichs, R. *Chem. Phys. Lett.* **1996**, *256*, 454.
(69) van Gisbergen, S. J. A.; Snijders, J. G.; Baerends, E. J. *Comput. Phys. Commun.* **1999**, *118*, 119.
(70) Stener, M.; Fronzoni, G.; de Simone, M. *Chem. Phys. Lett.* **2003**, *373*, 115.
(71) Montgomery, H.; Lingafelter, E. C. *Acta Crystallogr. B* **1968**, *24*, 1127.
(72) Garrett, T. P. J.; Guss, J. M.; Freeman, H. C. *Acta Crystallogr. C* **1983**, *39*, 1027.
(73) Cheng, C.-Y.; Wang, S.-L. *Acta Crystallogr. C* **1991**, *47*, 1734.
(74) Fackler, J. P., Jr.; Avdeef, A. *Inorg. Chem.* **1974**, *13*, 1864.
(75) Kessissoglou, D. P.; Li, X.; Butler, W. M.; Pecoraro, V. L. *Inorg. Chem.* **1987**, *26*, 2487.
(76) Larson, E.; Lah, M. S.; Li, X.; Bonadies, J. A.; Pecoraro, V. L. *Inorg. Chem.* **1992**, *31*, 373.
(77) Pavacik, P. S.; Huffman, J. C.; Christou, G. *J. Chem. Soc., Chem. Commun.* **1986**, 43.
(78) Thompson, M. A. *ArgusLab 4.0.0*; Planaria Software LLC: Seattle, WA, 2004.
(79) Te Velde, G.; Bickelhaupt, F. M.; Baerends, E. J.; Fonseca Guerra, C.; van Gisbergen, S. J. A.; Snijders, J. G.; Ziegler, T. *J. Comput. Chem.* **2001**, *22*, 931.
(80) Vosko, S. H.; Wilk, L.; Nusair, M. *Can. J. Phys.* **1980**, *58*, 1200.
(81) Becke, A. D. *Phys. Rev. A* **1988**, *38*, 3098.
(82) Perdew, J. P. *Phys. Rev. B* **1986**, *33*, 8822.
(83) van Lenthe, E.; Baerends, E. J. *J. Comput. Chem.* **2003**, *24*, 1142.
(84) van Lenthe, E.; Ehlers, A.; Baerends, E. J. *J. Chem. Phys.* **1999**, *110*, 8943.
(85) Krzystek, J.; Yeagle, G. J.; Park, J.-H.; Britt, R. D.; Meisel, M. W.; Brunel, L.-C.; Telser, J. *Inorg. Chem.* **2003**, *42*, 4610.
(86) Kessissoglou, D. P.; Butler, W. M.; Pecoraro, V. L. *J. Chem. Soc., Chem. Commun.* **1986**, 1253.
(87) Gohdes, J. W.; Armstrong, W. H. *Inorg. Chem.* **1992**, *31*, 368.
(88) van Leeuwen, R.; Baerends, E. J. *Phys. Rev. A* **1994**, *49*, 2421.
(89) Gross, E. K. U.; Kohn, W. *Adv. Quantum Chem.* **1990**, *21*, 255.
(90) Rosa, A.; Baerends, E. J.; van Gisbergen, S. J. A.; van Lenthe, E.; Groeneveld, J. A.; Snijders, J. G. *J. Am. Chem. Soc.* **1999**, *121*, 10356.
(91) Wang, F.; Ziegler, T. *Mol. Phys.* **2004**, *102*, 2585. *Phys.* **2005**, *122*, 204103.
(92) Kawai, J.; Mizutani, Y.; Sugimura, T.; Sai, M.; Higuchi, T.; Harada, Y.; Ishiwata, Y.; Fukushima, A.; Fujisawa, M.; Watanabe, M.; Maeda, K.; Shin, S.; Gohshi, Y. *Spectrochim. Acta B* **2000**, *55*, 1385.
(93) Richert, S. A.; Tsang, P. K. S.; Sawyer, D. T. *Inorg. Chem.* **1988**, *27*, 1814.
(94) Schipper, P. R. T.; Gritsenko, O. V.; van Gisbergen, S.; Baerends, E. J. *J. Chem. Phys.* **2000**, *112*, 1344.
(95) Grüning, M.; Gritsenko, O. V.; van Gisbergen, S.; Baerends, E. J. *J. Chem. Phys.* **2001**, *114*, 652.
(96) Ray, K.; DeBeer George, S.; Solomon, E. I.; Wieghardt, K.; Neese, F. *Chem. Eur. J.* **2007**, *13*, 2783.
(97) Wang, F.; Ziegler, T.; van Lenthe, E.; van Gisbergen, S.; Baerends, E. J. *J. Chem. Phys.* **2005**, *122*, 204103.
(98) Kirby, J. A.; Goodin, D. B.; Wydrzynski, T.; Robertson, A. S.; Klein, M. P. *J. Am. Chem. Soc.* **1981**, *103*, 5537.
(99) Imamura, Y.; Nakai, H. *Chem. Phys. Lett.* **2006**, *419*, 297.
(100) Fronzoni, G.; De Francesco, R.; Stener, M.; Causa, M. *J. Phys. Chem. B* **2006**, *110*, 9899.

JP803286C